

DOMAIN AGNOSTIC IMAGE-TO-IMAGE TRANSLATION USING LOW-RESOLUTION CONDITIONING

PREPRINT, COMPILED MAY 12, 2023

Mohamed Abid¹, Arman Afrasiyabi¹, Ihsen Hedhli¹, Jean-François Lalonde¹, and Christian Gagné^{1,2*}

¹Institute Intelligence and Data (IID), Université Laval

²Canada CIFAR AI Chair, Mila – Quebec AI Institute

ABSTRACT

Generally, image-to-image translation (i2i) methods aim at learning mappings across domains with the assumption that the images used for translation share content (e.g., pose) but have their own domain-specific information (a.k.a. style). Conditioned on a target image, such methods extract the target style and combine it with the source image content, keeping coherence between the domains. In our proposal, we depart from this traditional view and instead consider the scenario where the target domain is represented by a very low-resolution (LR) image, proposing a domain-agnostic i2i method for fine-grained problems, where the domains are related. More specifically, our domain-agnostic approach aims at generating an image that combines visual features from the source image with low-frequency information (e.g. pose, color) of the LR target image. To do so, we present a novel approach that relies on training the generative model to produce images that both share distinctive information of the associated source image and correctly match the LR target image when downscaled. We validate our method on the CelebA-HQ and AFHQ datasets by demonstrating improvements in terms of visual quality. Qualitative and quantitative results show that when dealing with intra-domain image translation, our method generates realistic samples compared to state-of-the-art methods such as StarGAN v2. Ablation studies also reveal that our method is robust to changes in color, it can be applied to out-of-distribution images, and it allows for manual control over the final results.

arXiv:2305.05023v2 [eess.IV] 11 May 2023

Under consideration in *Computer Vision and Image Understanding*.

*christian.gagne@gel.ulaval.ca

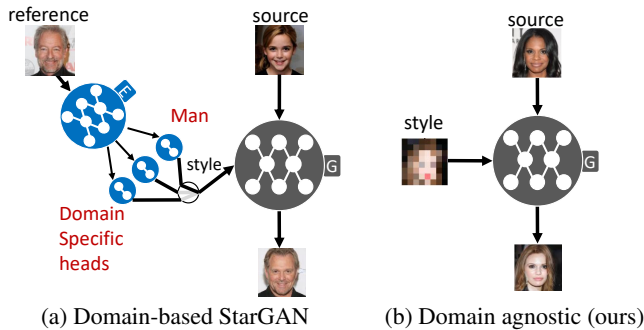


Figure 1: Comparison of StarGAN [Choi et al., 2018, 2020] as a conventional method with our domain-agnostic approach. While domain-based StarGAN (a) aims at extracting domain-specific style using a style encoder E from the reference image, our domain-agnostic approach (b) uses the low-resolution conditioning directly without requiring knowledge of a domain label.

1 INTRODUCTION

Image-to-image translation (i2i) methods seek to learn a mapping between two related domains, thereby “translating” an image from one domain to another while preserving some information from the original. These methods have been used for various applications in computer vision, such as colorization [Su et al., 2020], super-resolution [Ledig et al., 2017, Wang et al., 2018], medical imaging [Armanious et al., 2020], and photorealistic image synthesis [Zhang et al., 2017], achieving promising results both in terms of visual quality and diversity. Here, one key idea is to enforce the model to preserve the content of the image while modifying its style. This inspired many works such as Huang et al. [2018] and Lee et al. [2018] to disentangle the feature space into 1) a domain-specific space for the style; and 2) a shared space for the content—this allowed more diverse multimodal generation.

Recent methods such as StarGAN [Choi et al., 2018, 2020] unified the process in a single framework that works across many domains. These methods also introduced the problem of *conditional* image-to-image translation which aims at conditioning this process using a specific image from the target domain. As defined by Lin et al. [2018], conditional i2i “requires that the generated image should inherit some domain-specific features of the conditional image from the target domain”. Traditionally, methods aim to extract the style of a target image and merge it with the content of a source image to generate an image that shares information from both the source and target. Additionally, domain-specific information also guides the learning process. For instance, to translate an image from one domain to another domain, StarGAN [Choi et al., 2018, 2020] requires domain supervision in the form of a domain label.

In this work, we depart from this traditional view of conditional i2i and propose a novel perspective for domain-agnostic i2i. In particular, we consider the scenario where the “content” of an image is defined by its low-frequency information, while the “style” is defined by the high-frequency. Specifically, from an input source and a downsampled version of the target, we wish to recover an image that contains high-frequency information

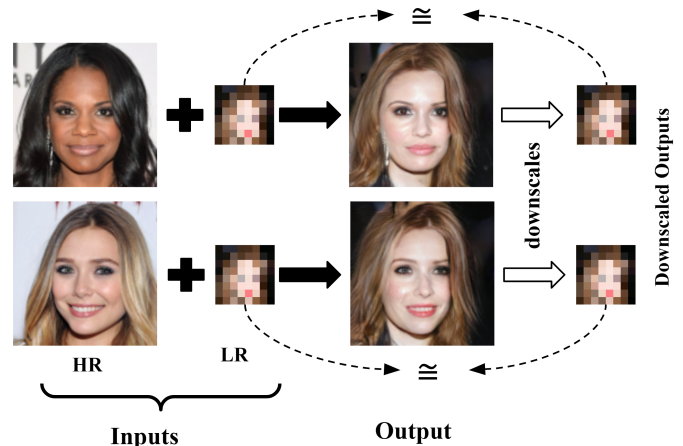


Figure 2: Illustration of the proposed approach on CelebA-HQ dataset: our method learned to map the inputs high-resolution image (HR, source) and low-resolution (LR, target) image to generate a HR output that preserves the identity of the source image and stays faithful to the structure of the LR target.

(details) from the source image while downscaling to the low-resolution (LR) target image. Contrarily to previous work, no target domain label is provided to the model: domain information is obtained directly from the target image itself. As illustrated in fig. 1-(a), conventional cross-domain supervised methods such as StarGAN [Choi et al., 2018, 2020] use a style encoder network E to extract a style vector from the reference image, which is then injected in the generator network G . In comparison and as shown in fig. 1-(b), our domain-agnostic approach is a fully unsupervised network across the domains, and our proposed algorithm only employs a single generator G network. As illustrated in fig. 2, the resulting learned mapping can generate an image that shares distinctive features from both the high-resolution (HR) source image and the LR target image in an unsupervised manner.

The main contribution of this paper is to define a novel domain-agnostic framework for fine-grained problems that can learn a mapping between images while being conditioned on the low-frequency information represented by a very low-resolution version of the target. Particularly, our method can perform i2i translation between domains without injecting label information, in a fully unsupervised manner. We demonstrate that our approach can effectively be used to transfer useful features (e.g., pose, spatial structure) from downsampled targets where details are completely blurred to the point of being visually unrecognizable. When evaluating our approach on the CelebA-HQ and AFHQ datasets, we show that our framework results in realistic samples according to the FID and LPIPS scores on both datasets. We also provide more evidence with our ablation study on a different aspect of our model. These extensive experiments demonstrate that our method can generate results that are photorealistic and that convincingly fuse information from both the HR source and LR target images. Finally, performed ablations show how our approach results in better image synthesis compared to StarGAN [Choi et al., 2018, 2020] under the same training settings.

2 RELATED WORK

Generative adversarial networks (GANs) [Goodfellow et al., 2014] are prominent generative methods with demonstrated results in various applications in computer vision, including image generation [Brock et al., 2018, Karras et al., 2019, 2020], super-resolution [Ledig et al., 2017, Wang et al., 2018, Kim et al., 2022b] and image-to-image translation [Hu et al., 2022, Huang et al., 2018, Kim et al., 2022a, Isola et al., 2017, Lee et al., 2018, Mao et al., 2019, Zhu et al., 2017, Kim et al., 2022a].

Some work has striven to improve sample quality and diversity, notably through theoretical breakthroughs in terms of defining loss functions that provide more stable training [Arjovsky et al., 2017, Gulrajani et al., 2017, Xudong et al., 2017, Zhao et al., 2017, Hoyer et al., 2022] and encourage diversity in the generated images [Mescheder et al., 2018, Yang et al., 2019]. Architectural innovations also played a crucial role in these advancements [Kim et al., 2019, Brock et al., 2018, Choi et al., 2020, Karras et al., 2018, Liu et al., 2017, Yang et al., 2022]. For instance, Liu et al. [2017] makes use of an attention layer that allows it to focus on long-range dependencies present in the image. Spectral normalization [Miyato et al., 2018] stabilizes the network, which also translates into having high-quality samples. Since our work sits at the intersection of reference-guided image synthesis and super-resolution, the remainder of this section focuses on these two branches exclusively.

Reference-guided image synthesis Also dubbed “conditional” [Lin et al., 2018], reference-guided i2i translation methods seek to learn a mapping from a source to a target domain while being conditioned on a specific image instance belonging to the target domain. In this case, some methods attempt to preserve the “content” of the source image (e.g., identity, pose) and apply the “style” (e.g., hair/skin color) of the target. Inspired by the mapping network of StyleGAN [Karras et al., 2019], recent methods [Choi et al., 2018, 2020, Huang et al., 2018] make use of a style encoder to extract the style of a target image and feed it to the generator, typically via adaptive instance normalization (AdaIN) [Huang and Belongie, 2017]. All these methods have the built-in assumption that the resolution of the source and target images are the same. In this work, the “style” of the target is preserved by conditioning on a LR version of the same target image.

Super-resolution Our approach bears some resemblance to super-resolution methods, which are aiming to learn a mapping from LR to a plausible HR images [Ledig et al., 2017, Dong et al., 2014], trained over ground truth HR images. More closely related are the so-called reference-guided super-resolution methods, which, in addition to the LR input image, also accept an additional HR images for guiding the generation process [Zheng et al., 2018, Zhang et al., 2019]. The critical difference is that, in this paper, we do not aim to recover the ground truth HR image. Rather, our method extracts distinctive information from the source image (HR) and generates an image which simultaneously: 1) contains this information; and 2) downscales to the target LR image.

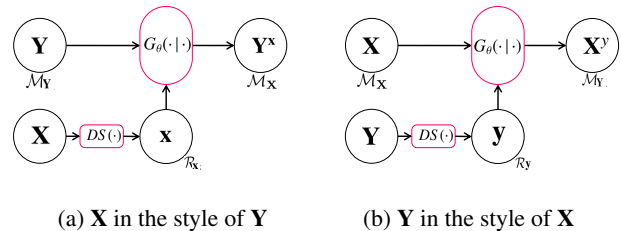


Figure 3: Illustration of our domain-agnostic method. Generator G_θ is trained to achieve a high-resolution mapping of a \mathbf{Y} (resp. \mathbf{X}) from its current domain \mathcal{M}_Y (resp. \mathcal{M}_X) to the target domain \mathcal{M}_X (resp. \mathcal{M}_Y), conditioned on \mathbf{x} , a low-resolution version of \mathbf{X} (resp. \mathbf{y} of \mathbf{Y}). (a) Translation of high-resolution image \mathbf{Y} from \mathcal{M}_Y to \mathcal{M}_X guided by \mathbf{x} , a low-resolution version of the target. (b) Generation of \mathbf{X}^Y , that correspond to \mathbf{X} in the style of \mathbf{Y} .

3 METHOD

To define the target domain, we are given a low-resolution (LR) version of the target image $\mathbf{x} \in \mathbb{R}^{m \times n}$, and we define the associated \mathcal{R}_x subspace of LR images as:

$$\mathcal{R}_x = \{ \forall i, \mathbf{x}_i \in \mathbb{R}^{m \times n} : \|\mathbf{x}_i - \mathbf{x}\|_p \leq \epsilon \}. \quad (1)$$

We consider an ϵ close to zero, so that each subspace contains only the LR images \mathbf{x}_i that are highly similar to the LR target \mathbf{x} according to a given norm p (here $p = 1$). We are also defining a target subspace \mathcal{M}_X in the source image manifold that includes all images that are included in \mathcal{R}_x when downsampled as LR images:

$$\mathcal{M}_X = \{ \forall j, \mathbf{X}_j \in \mathbb{R}^{M \times N} : DS(\mathbf{X}_j) \in \mathcal{R}_x \}, \quad (2)$$

where \mathbf{X}_j is an image in the high-resolution (HR) space, and $DS(\cdot)$ is a downsampling operator. As in Berthelot et al. [2020], average pooling is used for downsampling with $DS(\cdot)$. Therefore, for each subspace \mathcal{M}_X , there exists a corresponding subspace \mathcal{R}_x in the LR space related by $DS(\cdot)$. As illustrated in fig. 3, given two pairs $(\mathbf{X} \in \mathcal{M}_X, \mathbf{x} = DS(\mathbf{X}))$ and $(\mathbf{Y} \in \mathcal{M}_Y, \mathbf{y} = DS(\mathbf{Y}))$, our goal is to learn a domain agnostic function G that translates the source images from one subspace \mathcal{M}_X to another subspace \mathcal{M}_Y . These two subspaces are defined according to information provided by their LR target version counterpart (i.e., \mathcal{R}_x and \mathcal{R}_y , respectively):

$$\begin{aligned} G : \mathcal{M}_Y \times \mathcal{R}_x &\mapsto \mathcal{M}_X, G_\theta(\mathbf{Y} | \mathbf{x}), \\ G : \mathcal{M}_X \times \mathcal{R}_y &\mapsto \mathcal{M}_Y, G_\theta(\mathbf{X} | \mathbf{y}). \end{aligned} \quad (3)$$

As shown in fig. 3 (b), in practice, we follow a straightforward learning algorithm for our proposed domain-agnostic approach. For example, our domain-agnostic approach outputs \mathbf{X}^Y which is the translation of HR input image \mathbf{X} in the style of \mathbf{y} . To this end, we employ the generator G_θ network parameterized by θ .

Following conventional GAN terminology [Goodfellow et al., 2020], parameterized function G_θ is a generator (simplified as G hereinafter) which aims at translating a source image from a subspace to a target subspace while preserving distinctive source features. Training G relies on a discriminator D that plays two roles: 1) to classify whether the generated images are

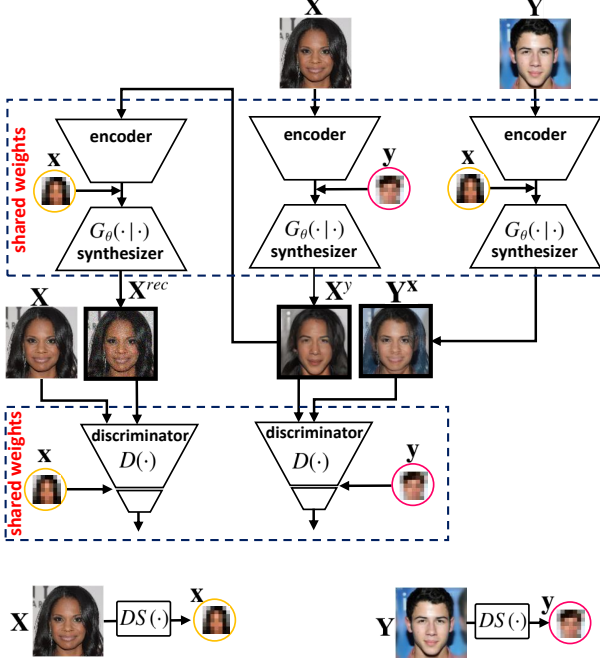


Figure 4: Schematic overview of our training algorithm to obtain \mathbf{X}^y (resp. \mathbf{Y}^x) which corresponds to translating image \mathbf{X} (resp. \mathbf{Y}) to the target domain of image \mathbf{Y} (resp. \mathbf{X}) based on its low resolution version \mathbf{y} (resp. \mathbf{x}). Generator G_θ translates high resolution input images using low resolution versions of the target domain images. Besides, network D_ϕ aims at discriminating between \mathbf{X}^y and \mathbf{Y}^x , and between the reconstructed $\mathbf{X}^{rec} = G_\theta(\mathbf{X}^y | \mathbf{x})$ version of \mathbf{X}^y and the original \mathbf{X} . The networks inside each dashed box (labeled with shared weights) are the same. The low resolution versions of the input images \mathbf{x} and \mathbf{y} are obtained using a non-parametric function $DS(\cdot)$ function applied on \mathbf{X} and \mathbf{Y} , respectively.

fake or real, pushing G to generate samples on the natural image manifold; and 2) to evaluate whether the translated source image is part of the right target domain according to the downsampling constraint.

3.1 Training Objectives

For achieving these two discrimination roles, the GAN is trained according to the following minimax optimization:

$$\min_G \max_D \mathcal{L}_{adv} + \lambda_{cyc} \mathcal{L}_{cyc}, \quad (4)$$

where \mathcal{L}_{adv} is an adversarial loss used to ensure that we are generating plausible natural images, \mathcal{L}_{cyc} is the cycle consistency loss ensuring that the translated images are kept on the correct subspace while carrying the right features, and λ_{cyc} is a hyperparameter to achieve the right balance between these two losses. The process of translating \mathbf{X} in the style of \mathbf{Y} is illustrated in fig. 4. First, we translate \mathbf{X} (resp. \mathbf{Y}) using the parameterized generator, that is $\mathbf{X}^y = G_\theta(\mathbf{X} | \mathbf{y})$ (resp. $\mathbf{Y}^x = G_\theta(\mathbf{Y} | \mathbf{x})$). Then, we compute the reconstructed $\mathbf{X}^{rec} = G_\theta(\mathbf{X}^y | \mathbf{x})$ version of \mathbf{X} . Finally, the resulting images are feedforwarded twice through discriminator $D_\phi(\cdot)$: 1) to determine which image between \mathbf{X}^y and \mathbf{Y}^x are conditioned on the low resolution \mathbf{x} , and

Algorithm 1: Domain-agnostic image-to-image translation from low-resolution conditioning

Data: Generator $G_\theta(\cdot | \cdot)$, discriminator $D_\phi(\cdot)$, downsampling function $DS(\cdot)$, training dataset \mathcal{X}_{train} , learning rate η , maximum number of training iterations t^{max} .

```

for  $t = 1, \dots, t^{max}$  do
    # Pick a random pair of samples and their low-resolution
    sample  $\mathbf{X} \in \mathcal{X}_{train}$  and  $\mathbf{Y} \in \mathcal{X}_{train}$ 
     $\mathbf{x} = DS(\mathbf{X})$ ;  $\mathbf{y} = DS(\mathbf{Y})$ 
    # Feedforward samples through generator
     $\mathbf{X}^y = G_\theta(\mathbf{X} | \mathbf{y})$ ;  $\mathbf{Y}^x = G_\theta(\mathbf{Y} | \mathbf{x})$ 
     $\mathbf{X}^{rec} = G_\theta(\mathbf{X}^y | \mathbf{x})$ ;  $\mathbf{Y}^{rec} = G_\theta(\mathbf{Y}^x | \mathbf{y})$ 
    Compute adversarial  $\mathcal{L}_{adv}$  loss in the form of Eq. 8
    # Update discriminator with adversarial loss
     $\phi \leftarrow \phi - \eta \nabla_\phi \mathcal{L}_{adv}$ 
    Compute cycle loss  $\mathcal{L}_{cyc}$  using Eq. 9
    # Compute reconstruction loss using  $l_1$  norm
     $\mathcal{L}_{rec} = \|\mathbf{X} - \mathbf{X}^{rec}\|_1 + \|\mathbf{Y} - \mathbf{Y}^{rec}\|_1$ 
    # Update generator with cycle and reconstruction losses
     $\theta \leftarrow \theta - \eta \nabla_\theta (\mathcal{L}_{cyc} + \mathcal{L}_{rec})$ 
end
    
```

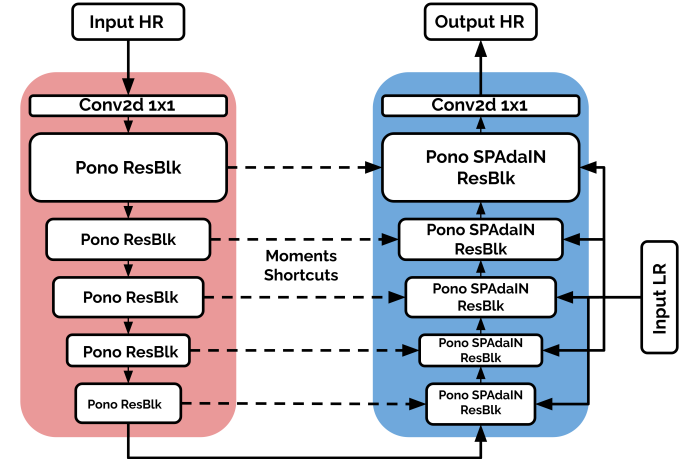


Figure 5: Generator architecture: the encoding part (in red) is used for extracting structural information in the source image, which is merged in the decoder (in blue) with the incoming features from the decoding output and the low resolution targets.

2) to discriminate between \mathbf{X} and its corresponding reconstruction \mathbf{X}^{rec} .

At each training iteration, four forward passes are done with the generator: the first two for generating $\mathbf{X}^y = G_\theta(\mathbf{X} | \mathbf{y})$ and $\mathbf{Y}^x = G_\theta(\mathbf{Y} | \mathbf{x})$, while the other two are for cycle consistency (i.e., $G_\theta(G_\theta(\mathbf{X} | \mathbf{y}) | \mathbf{x}) \approx \mathbf{X}$ and $G_\theta(G_\theta(\mathbf{Y} | \mathbf{x}) | \mathbf{y}) \approx \mathbf{Y}$). The discriminator is used to make sure that the generated samples are from the designated subspace.

Adversarial loss Following Berthelot et al. [2020], we provide the discriminator with the absolute difference $\mathbf{d}_{\mathbf{X} \rightarrow \mathcal{M}_Y} \in \mathbb{R}^{m \times n}$ between the downscaled version of the generated image $DS(G_\theta(\mathbf{X} | \mathbf{y}))$ and the LR target $\mathbf{y} = DS(\mathbf{Y})$:

$$\mathbf{d}_{\mathbf{X} \rightarrow \mathcal{M}_Y} = \frac{|\mathbf{y} - \lfloor r DS(G_\theta(\mathbf{X} | \mathbf{y})) \rfloor|}{r}, \quad (5)$$

where r is the color resolution. As in Berthelot et al. [2020], we round the downsampled image to its nearest color resolution ($r = 2/255$, since pixel values are in $[-1, 1]$) to avoid unstable optimization caused by exceedingly large weights to measure small pixel value differences. A straight-through estimator [Bengio et al., 2013] is employed to pass the gradient through the rounding operation in eq. 5. The discriminator, therefore, takes as inputs:

$$\begin{cases} D_\phi(\mathbf{Y}, \mathbf{0}) & \text{for real samples,} \\ D_\phi(G_\theta(\mathbf{X}|\mathbf{y}), \mathbf{d}_{\mathbf{X} \rightarrow \mathcal{M}_Y}) & \text{otherwise.} \end{cases} \quad (6)$$

Here, $\mathbf{0}$ is an all-zeros $m \times n$ image difference, since the downsampled version of \mathbf{Y} is exactly \mathbf{y} . However, for fake samples, the absolute difference $\mathbf{d}_{\mathbf{X} \rightarrow \mathcal{M}_Y}$ depends on how close is the generator to the designated subspace, \mathcal{M}_Y in our example. Both networks G and D are trained via the resulting adversarial loss:

$$\begin{aligned} \mathcal{L}_{\text{adv}}(\mathbf{X}, \mathbf{Y}) = & \log D_\phi(\mathbf{X}, \mathbf{0}) + \log D_\phi(\mathbf{Y}, \mathbf{0}) \\ & + \log(1 - D_\phi(G_\theta(\mathbf{X}|\text{DS}(\mathbf{Y})), \mathbf{d}_{\mathbf{X} \rightarrow \mathcal{M}_Y})) . \end{aligned} \quad (7)$$

In the same manner, we compute the adversarial loss between $(\mathbf{X}, \mathbf{Y}^x)$, $(\mathbf{X}, \mathbf{X}^{\text{rec}})$, $(\mathbf{Y}, \mathbf{Y}^y)$, and $(\mathbf{Y}, \mathbf{Y}^{\text{rec}})$ pairs, respectively. Finally, we compute the overall adversarial loss \mathcal{L}_{adv} in the following form:

$$\begin{aligned} \mathcal{L}_{\text{adv}} = & \mathcal{L}_{\text{adv}}(\mathbf{X}, \mathbf{Y}^x) + \mathcal{L}_{\text{adv}}(\mathbf{X}, \mathbf{X}^{\text{rec}}) \\ & + \mathcal{L}_{\text{adv}}(\mathbf{Y}, \mathbf{Y}^y) + \mathcal{L}_{\text{adv}}(\mathbf{Y}, \mathbf{Y}^{\text{rec}}) . \end{aligned} \quad (8)$$

Cycle consistency loss To make sure that generator G preserves the distinctive features available in the source image, we employ the cycle consistency constraint [Isola et al., 2017, Liu et al., 2017, Zhu et al., 2017] in both directions, each time by changing the LR target to specify the designated subspace:

$$\begin{aligned} \mathcal{L}_{\text{cyc}}(\mathbf{X}, \mathbf{Y}) = & \|\mathbf{X} - G_\theta(G_\theta(\mathbf{X}|\text{DS}(\mathbf{Y}))|\text{DS}(\mathbf{X}))\|_1 \\ & + \|\mathbf{Y} - G_\theta(G_\theta(\mathbf{Y}|\text{DS}(\mathbf{X}))|\text{DS}(\mathbf{Y}))\|_1 . \end{aligned} \quad (9)$$

Likewise, we compute the cycle loss between $(\mathbf{X}, \mathbf{Y}^x)$, $(\mathbf{X}, \mathbf{X}^{\text{rec}})$, $(\mathbf{X}, \mathbf{X}^{\text{rec}})$, $(\mathbf{Y}, \mathbf{Y}^y)$, and $(\mathbf{Y}, \mathbf{Y}^{\text{rec}})$. Finally, we compute the overall adversarial loss \mathcal{L}_{cyc} in the following form:

$$\begin{aligned} \mathcal{L}_{\text{cyc}} = & \mathcal{L}_{\text{cyc}}(\mathbf{X}, \mathbf{Y}^x) + \mathcal{L}_{\text{cyc}}(\mathbf{X}, \mathbf{X}^{\text{rec}}) \\ & + \mathcal{L}_{\text{cyc}}(\mathbf{Y}, \mathbf{Y}^y) + \mathcal{L}_{\text{cyc}}(\mathbf{Y}, \mathbf{Y}^{\text{rec}}) \end{aligned} \quad (10)$$

This cycle consistency loss encourages the generator to identify the shared and invariant information between every two subspaces for preserving it during translation. Alg. 1 illustrates how we feedforward through the generator G_θ and the discriminator D_ϕ and compute the losses during our proposed domain-agnostic i2i approach.

3.2 Architecture

Most current image-to-image translation models [Choi et al., 2018, Huang et al., 2018] rely on Adaptive Instance Normalization (AdaIN) [Huang and Belongie, 2017, Karras et al., 2019] to transfer the style from a reference image to a source image. However, in our work the hypothesis of content and style is not suitable since the LR image contains information on both style (e.g., colors) and content (e.g., pose). Thus, our generator adapts source image to the content and style of the LR image through the use of spatially adaptive instance normalization (SPAdaIN) [Wang et al., 2020].

Generator G (fig. 5) is U-shaped, with skip connections (a.k.a. moments shortcuts in Li et al. [2019]) between the encoding and decoding part. The encoder takes the input image, passes it through a series of downsampling residual blocks (ResBlks) [He et al., 2016]. Each ResBlks is equipped with instance normalization (IN) to remove the style of the input, followed by 2D convolution layers and a positional normalization (Pono) [Li et al., 2019]. The mean μ and variance σ are subtracted and passed as a skip connection to the corresponding block in the decoder. Pono and moments shortcuts plays a crucial role in transferring the needed structural information from the source image to the decoding part of the network. These blocks, dubbed *Pono ResBlks*, are illustrated in detail in fig. 6 (a).

For the decoder blocks shown in fig. 6(b), we use SPAdaIN [Wang et al., 2020] conditioned on the LR image, where the LR image is first upsampled to the corresponding resolution of the *Pono SPAdaIN ResBlk* using bilinear upsampling. It is then followed by 2D convolution layers and a dynamic moment shortcut layer, where, instead of reinjecting μ and σ as is, we use a convolutional layer that takes μ and σ as inputs to generate the β and γ used as moment shortcuts. Using the dynamic version of moment shortcuts [Li et al., 2019] allows the network to adapt and align the shape of the incoming structural information to its LR counterpart.

We use the StarGAN v2 [Choi et al., 2020] discriminator architecture without the domain-specific layers since we do not have predefined domains. We also concatenate the image difference (eq. 5) at the corresponding layer (same height and width).

4 EXPERIMENTS

Baseline We compare our method with StarGAN v2 [Choi et al., 2020], the state-of-the-art for image-to-image generation on CelebA-HQ and AFHQ. However, since previous i2i methods do not make use of LR images, the comparison is provided to illustrate the differences and the advantages of each method.

Datasets We evaluate our method on the CelebA-HQ [Karras et al., 2018] and AFHQ [Choi et al., 2020] datasets. However, for CelebA-HQ we do not separate the two domains into female and male since both domains are close to each other. Also, we are not using any extra information (e.g., facial attributes of CelebA-HQ). For AFHQ, we train our network on each domain separately (i.e., cats, dogs and wild), since the amount of information shared between these is much lower.

Evaluation metrics Baseline results are evaluated according to the metrics of image-to-image translation used in Huang et al. [2018], Lee et al. [2018], Mao et al. [2019]. Specifically, diversity and visual quality of samples produced by different methods are evaluated both with the Fréchet inception distance (FID) [Heusel et al., 2017] and the learned perceptual image patch similarity (LPIPS) [Zhang et al., 2018].

4.1 Training Setup

For our experiments, we fixed the LR image resolution to 8×8 and experimented with 128×128 and 256×256 for the HR image resolution—we ablate the effect of LR image resolution

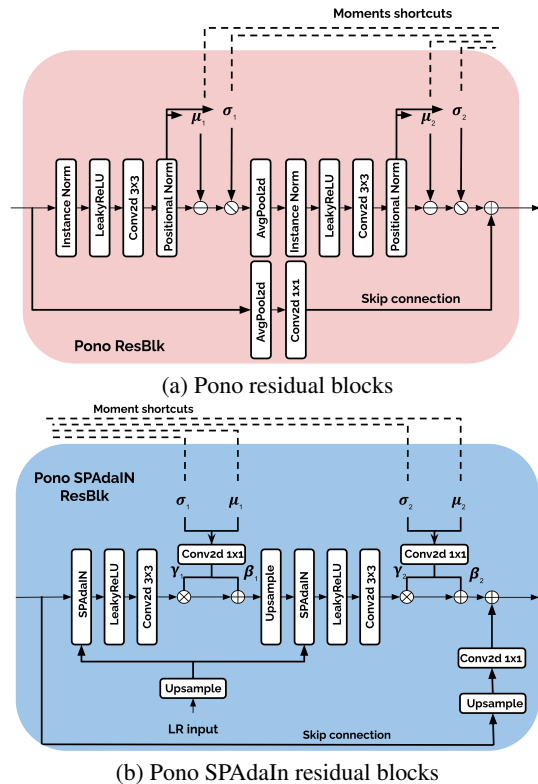


Figure 6: Residual blocks used in the generator G : (a) Encoding pono residual blocks, used to extract and compress the features coming from the source image and pass it to the decoding part of the generator through moments shortcuts and as compressed features; and (b) Decoding pono SPAdaIn residual blocks, which are taking as input extracted features from the encoding part, and also are upsampling the LR target image and pass it to the SPAdaIn layer [Wang et al., 2020].

in sec. 4.4. We train our networks with Adam [Kingma and Ba, 2015] and TTUR [Heusel et al., 2017], with a learning rate of 10^{-3} for the generator and 4×10^{-3} for the discriminator. We also used R^1 regularization [Mescheder et al., 2018] with $\gamma = 0.5$, with a batch size of 8. Spectral normalization [Miyato et al., 2018] was used in all the layers of both G and D . In eq. (1), we use $\epsilon = 0$ to push the downscaled version of the generated image to be as close as possible to the LR target. We set $\lambda_{cyc} = 1$ when trained on 128×128 , and to $\lambda_{cyc} = 0.1$ for 256×256 .

4.2 Qualitative Evaluation

Fig. 8 compares images obtained with our framework with those obtained with StarGAN v2 [Choi et al., 2020] using reference-guided synthesis on CelebA-HQ. Since our method focuses on generating images that downscale to the given LR image, the generator learns to merge the high frequency information presents in the source image with the low frequency information of the LR target, while preserving the identity of the person and other distinctive features. Differently from traditional i2i methods that only change the style of the source image while preserving its content, our method adapts the source image to the pose of the LR target. More qualitative samples

HR image res. Metric	128 × 128		256 × 256	
	FID \downarrow	LPIPS \uparrow	FID \downarrow	LPIPS \uparrow
MUNIT [Huang et al., 2018]	–	–	107.1	0.176
DRIT [Lee et al., 2018]	–	–	53.3	0.311
MSGAN [Mao et al., 2019]	–	–	39.6	0.312
StarGAN v2 [Choi et al., 2020]	19.58	0.22	23.8	0.38
Ours	15.52	0.34	25.89	0.329

Table 1: Quantitative comparison on the CelebA dataset, comparing our method to other reference-guided i2i methods [Choi et al., 2020, Huang et al., 2018, Lee et al., 2018, Mao et al., 2019]. We follow same procedure as in StarGAN v2 [Choi et al., 2020], but for our method we sample ten HR images for each LR image.

obtained with our technique are shown in fig. 7, where the first row of HR images are used as source images and the first column is the LR target. We also display the real HR target to show that our model is capable of generating diverse images that are different from the target.

Fig. 10 displays generated samples on AFHQ. Visually, we notice that our model is capable of merging most of the high frequency information coming from HR source image with low frequency information present in the LR target. The degree of this transfer depends on how much information is shared between the domain.

4.3 Quantitative Evaluation

In tab. 1, we report FID and LPIPS scores on the results obtained on CelebA-HQ, using two different resolutions, 128×128 and 256×256 . Results with the 256×256 resolution show a significantly lower FID of our method compared to Huang et al. [2018], Lee et al. [2018], Mao et al. [2019], while being similar to StarGAN v2 [Choi et al., 2020]. We notice a better FID score with the lower 128×128 resolution. This is due to the fact that the task is harder with higher scale factor since we need to hallucinate more detailed textural information missing from the LR target.

We also report quantitative results on AFHQ [Choi et al., 2020] in tab. 2, where we train our model on each domain separately given the higher differences of the domains distributions. Indeed, we found that our method excels on domains where images are structurally similar and share information, such as the “cats” domain. However, the “dogs” and “wild” domains show a wider variety of races and species, meaning less information shared between images from the same domain. This reduces the amount of shared information that can be transferred from the HR source, forcing to hallucinate more details out of LR targets. This is confirmed by the lower LPIPS results obtained by our approach compared to StarGAN v2, while keeping similar FID scores.

4.4 Ablation

To investigate the robustness of our method, we report the results on the impact of resolution, the effect of grayscale LR targets and the effect of added Gaussian noise on the generation process.

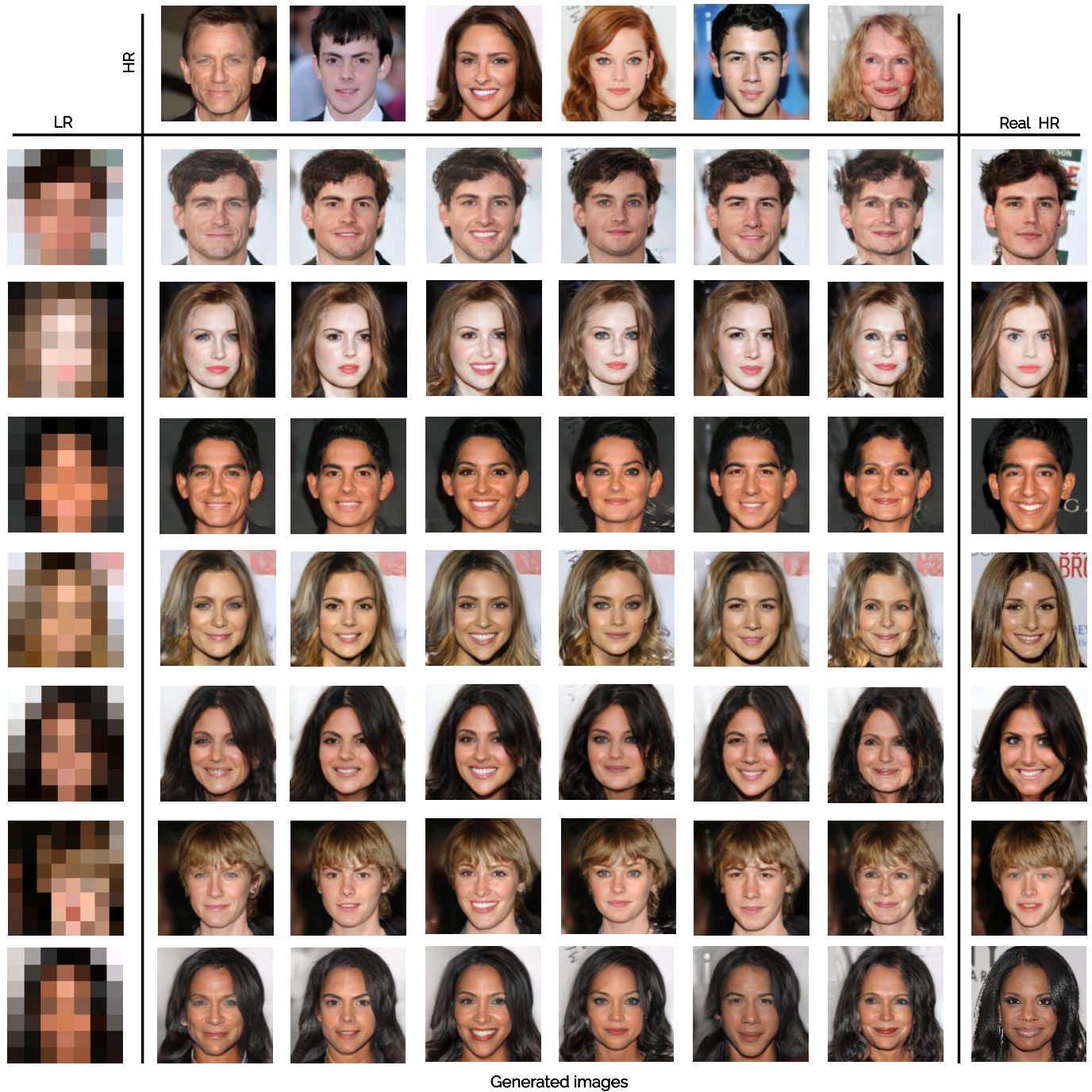


Figure 7: Qualitative reference-guided image synthesis results on CelebA-HQ. Our method takes the HR source images (top row), and translates them according to the LR target (left column). We also add the real HR target (not seen by the network) for visual comparison. See supplementary material for more results.

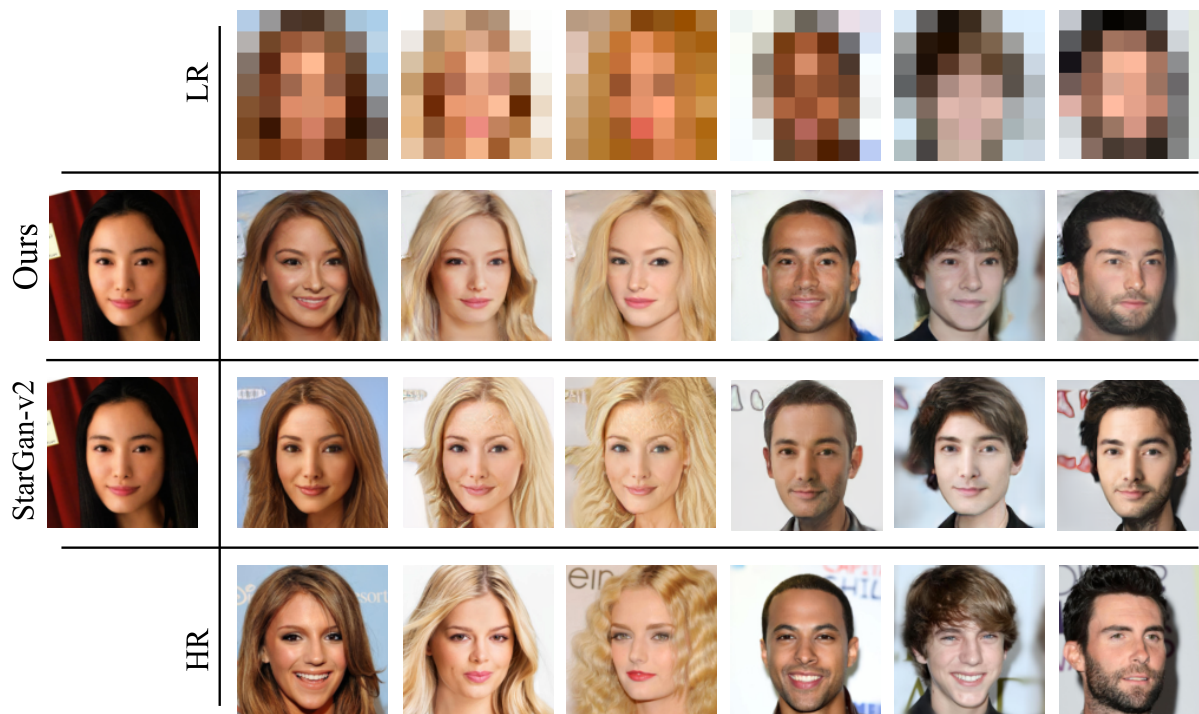


Figure 8: Comparison between our method and reference guided StarGAN v2 [Choi et al., 2020] on CelebA-HQ. For both methods, we use the same HR image as the source (left column). For the reference image, our method uses the LR images (top row) while StarGAN v2 [Choi et al., 2020] uses the corresponding HR (bottom row).

Impact of resolution Tab. 3 illustrates the impact of LR resolution on CelebA-HQ. As the LR target resolution increases, the model exploits the information in the LR target more and more over the information provided by the HR source image. This is confirmed by a sustained decrease in the LPIPS score when the resolution increases from 8×8 to 32×32 , while maintaining a similar FID score.

Impact of grayscale LR target Although our method is solely trained on RGB images, we tested our method on grayscale images (broadcasting the grayscale image 3 times along the channel axis) from CelebA-HQ dataset to investigate its impact on the SPadaIN module responsible for style guidance. We found that our model is robust to such effect and can successfully generate realistic grayscale images using HR source images.

Impact of Gaussian noise We added Gaussian noise to the LR target image with varying σ and found that the model is robust to $\sigma < 0.12$, see fig. 11. Even with $\sigma > 0.10$, the model preserved well the source image features and the identity of the face.

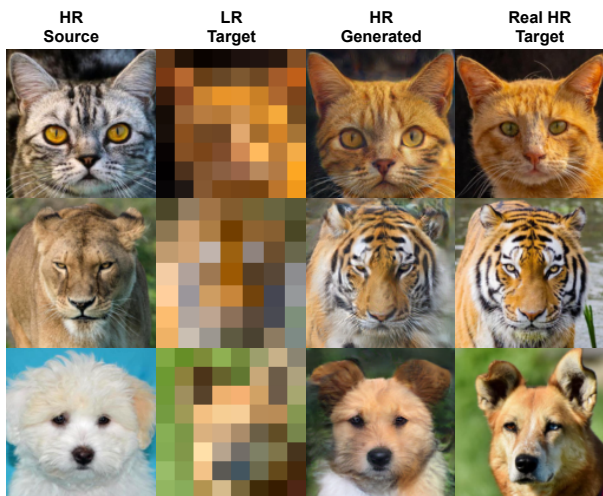


Figure 9: Qualitative results on the AFHQ dataset. Our method takes the HR images, and translate them to the corresponding HR subspace of the given LR target images. See supplementary material for more results.

4.5 Manual guidance

We show that our method can allow for manual controlled generation with fairly minimal changes in the LR target image. fig. 13 shows that manually altering pixel values in the LR image (beard) can generate a realistic change in the output.

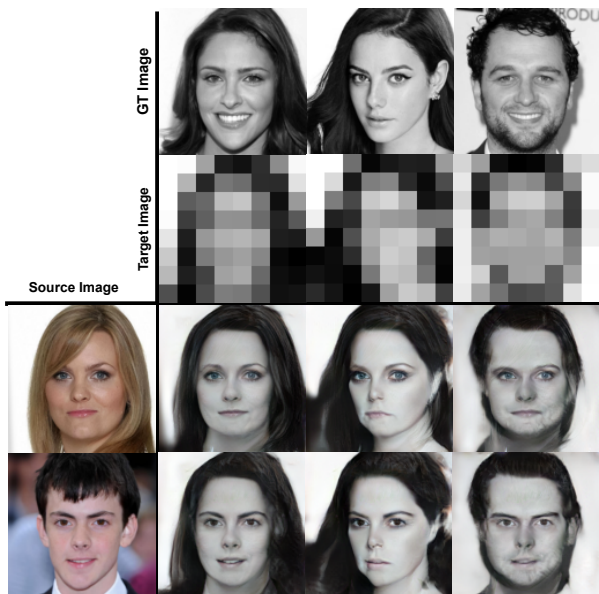


Figure 10: Results of using grayscale LR target to guide the generation process.

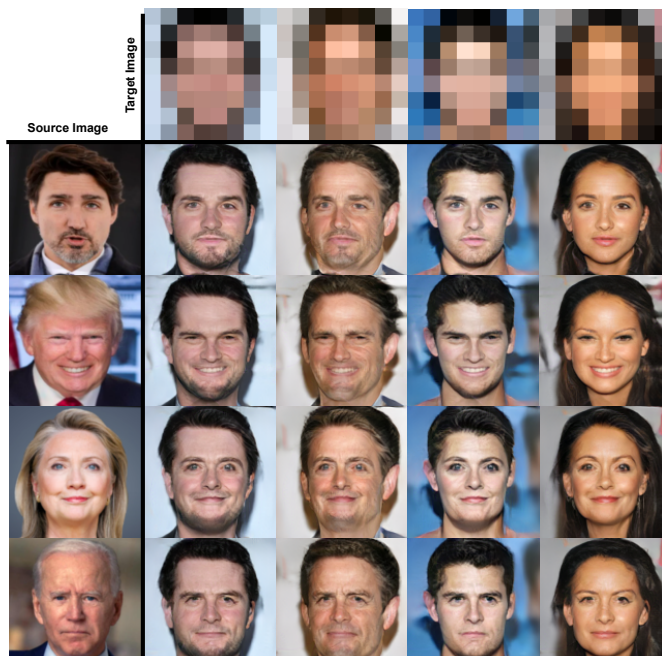


Figure 12: Qualitative results on politician faces that are not part of CelebA-HQ. Our method, trained on CelebA-HQ, takes the HR images as input and translates them to the corresponding HR subspace of the given LR target images.

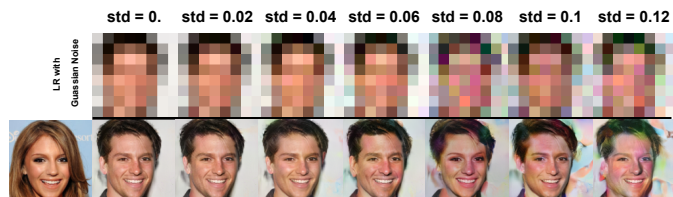


Figure 11: Qualitative results with added Gaussian noise to the LR target images.

Category Metric	Cats		Dogs		Wild	
	FID _↓	LPIPS _↑	FID _↓	LPIPS _↑	FID _↓	LPIPS _↑
StarGAN v2	25.2	0.42	56.5	0.34	19.87	0.46
Ours	22.8	0.40	67.3	0.47	20.61	0.23

Table 2: Quantitative comparison on the AFHQ dataset. We compare our method to the reference-guided i2i methods StarGAN v2 [Choi et al., 2020] where the target and the source image are from the same domain.

LR target res.	4 × 4	8 × 8	16 × 16	32 × 32
FID _↓	15.13	15.34	19.45	13.55
LPIPS _↑	0.30	0.34	0.14	0.08

Table 3: Effect of the LR resolution on the FID and LPIPS metrics for the CelebA-HQ dataset.

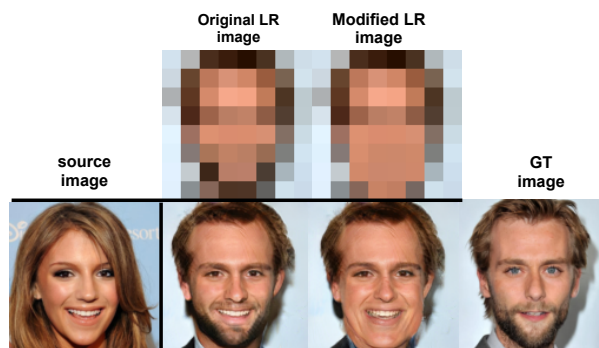


Figure 13: Image generation (bottom row) can be guided by manually altering the LR target image (top row).

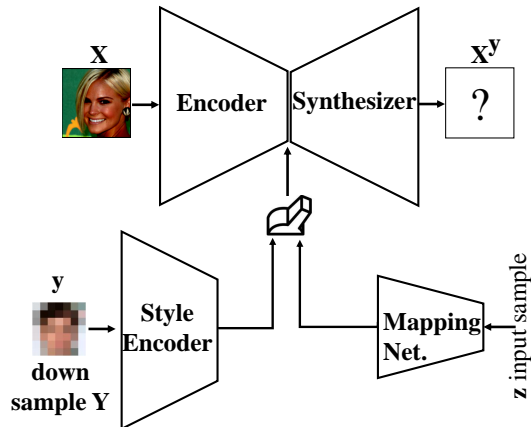


Figure 14: StarGAN v2 conditioned on LR. We ablate StarGAN v2 under two setups with and without a mapping network while the style encoder takes the LR input image.

4.6 StarGAN v2 under same setup

Unlike StarGAN v2 [Choi et al., 2020] with two additional learning modules besides generator and discriminator, our proposed model is domain-agnostic. Nevertheless, StarGAN v2 is still the most related work to our proposed model from i2i perspective. Therefore, we perform an ablative analysis of StarGAN v2 under the LR conditioning hypothesis, as shown in fig. 14. Particularly, we train the model by LR images as the input of the Style encoder. First, we kept the original architecture of StarGAN v2 and only conditioned the input of the style network on LR input image. Second, we train StarGAN v2 with LR inputs to style the network and without the mapping network to reduce one of the extra modules used in the original paper. As depicted in fig. fig. 15, StarGAN v2 struggles to produce realistic images when subjected to conditions akin to our domain-agnostic image-to-image translation.

5 DISCUSSION

This paper proposes a novel framework for reference-guided image synthesis. Our method attempts to realistically project the source images to a subspace of images that shares same features with a low resolution target (such as overall color distribution and pose). Our experiments show that our method allows for the generation of a wide variety of realistic images given LR targets. We validate our method on two well-known datasets, CelebA-HQ and AFHQ and we present its difference and advantages compared to the leading i2i methods Choi et al. [2020], Huang et al. [2018], Lee et al. [2018]. We also investigated the robustness of our method in terms of flexibility using grayscale images and its generalization on new faces outside of the dataset it is trained on. We also show that our method allows for a manual guidance with fairly minimal changes, such guidance can be intuitive and can be made directly on the LR target.



Figure 15: Examining the qualitative outcomes of conditioning StarGAN v2 using low-resolution images, in order to assess the proficiency of StarGAN v2 within the context of our domain-agnostic image-to-image translation. Here, we consider two versions of StarGAN v2, without a mapping network (top three rows) and with a mapping network (down three rows).

5.1 Limitations and future work

The main limitation of our method is that it assumes the target and source images come from the same distribution (e.g., human faces). In the case where these domains differ (e.g., tiger vs lion in the wild category of AFHQ), the generated image attempts to match the LR target at the expense of “forgetting” more information from the source image (fig. 10). A potential solution to mitigate this problem would be to soften the constraint of having to perfectly match the LR image, for instance by increasing the distance ϵ in eq. (1), or by modifying the discriminator inputs (eq. (6)) to tolerate larger differences. Finally, the framework has so far only been tested on faces (humans and animals). Extending it to handle more generic scenes, where the LR target would capture higher level information such as layout, makes for an exciting future research direction.

ACKNOWLEDGEMENTS

This work was done in the context of a collaborative R&D project with Thales Canada, which provided expertise, resources, support and funding. The project has been funded by the Natural Sciences and Engineering Research Council of Canada (NSERC) (RDPCJ 537836-18).

REFERENCES

Martin Arjovsky, Soumith Chintala, and Léon Bottou. Wasserstein generative adversarial networks. In *International Con-*

- ference on Machine Learning (ICML)*, 2017. URL <https://proceedings.mlr.press/v70/arjovsky17a.html>.
- Karim Armanious, Chenming Jiang, Marc Fischer, Thomas Küstner, Tobias Hepp, Konstantin Nikolaou, Sergios Gatidis, and Bin Yang. MedGAN: Medical image translation using GANs. *Computerized medical imaging and graphics*, 79:101684, 2020. URL <https://doi.org/10.1016/j.compmedig.2019.101684>.
- Yoshua Bengio, Nicholas Léonard, and Aaron C. Courville. Estimating or propagating gradients through stochastic neurons for conditional computation. *arXiv preprint arXiv:1308.3432*, 2013. URL <https://arxiv.org/abs/1308.3432>.
- David Berthelot, Peyman Milanfar, and Ian Goodfellow. Creating high resolution images with a latent adversarial generator. *arXiv preprint arXiv:2003.02365*, 2020. URL <https://arxiv.org/abs/2003.02365>.
- Andrew Brock, Jeff Donahue, and Karen Simonyan. Large scale GAN training for high fidelity natural image synthesis. In *International Conference on Learning Representations (ICLR)*, 2018. URL <https://arxiv.org/abs/1809.11096>.
- Yunjey Choi, Minje Choi, Munyoung Kim, Jung-Woo Ha, Sunghun Kim, and Jaegul Choo. StarGAN: Unified generative adversarial networks for multi-domain image-to-image translation. In *IEEE Conference on Computer Vision and Pattern Recognition (CVPR)*, 2018. URL https://openaccess.thecvf.com/content_cvpr_2018/html/Choi_StarGAN_Unified_Generative_CVPR_2018_paper.html.
- Yunjey Choi, Youngjung Uh, Jaejun Yoo, and Jung-Woo Ha. StarGAN v2: Diverse image synthesis for multiple domains. In *IEEE/CVF Conference on Computer Vision and Pattern Recognition (CVPR)*, 2020. URL https://openaccess.thecvf.com/content_CVPR_2020/html/Choi_StarGAN_v2_Diverse_Image_Synthesis_for_Multiple_Domains_CVPR_2020_paper.html.
- Chao Dong, Chen Change Loy, Kaiming He, and Xiaoou Tang. Learning a deep convolutional network for image super-resolution. In *European Conference on Computer Vision (ECCV)*, 2014. URL https://doi.org/10.1007/978-3-319-10593-2_13.
- Ian Goodfellow, Jean Pouget-Abadie, Mehdi Mirza, Bing Xu, David Warde-Farley, Sherjil Ozair, Aaron Courville, and Yoshua Bengio. Generative adversarial nets. In *Advances in Neural Information Processing Systems (NIPS)*, 2014. URL <https://arxiv.org/abs/1406.2661>.
- Ian Goodfellow, Jean Pouget-Abadie, Mehdi Mirza, Bing Xu, David Warde-Farley, Sherjil Ozair, Aaron Courville, and Yoshua Bengio. Generative adversarial networks. *Communications of the ACM*, 63(11):139–144, 2020. URL <https://dl.acm.org/doi/abs/10.1145/3422622>.
- Ishaan Gulrajani, Faruk Ahmed, Martin Arjovsky, Vincent Dumoulin, and Aaron C Courville. Improved training of Wasserstein GANs. In *Advances in Neural Information Processing Systems (NeurIPS)*, 2017. URL https://proceedings.neurips.cc/paper_files/paper/2017/hash/892c3b1c6dccc52936e27cbd0ff683d6-Abstract.html.
- Kaiming He, Xiangyu Zhang, Shaoqing Ren, and Jian Sun. Deep residual learning for image recognition. In *IEEE Conference on Computer Vision and Pattern Recognition (CVPR)*, 2016. URL https://openaccess.thecvf.com/content_cvpr_2016/html/He_Deep_Residual_Learning_CVPR_2016_paper.html.
- Martin Heusel, Hubert Ramsauer, Thomas Unterthiner, Bernhard Nessler, and Sepp Hochreiter. GANs trained by a two time-scale update rule converge to a local nash equilibrium. In *Advances in Neural Information Processing Systems (NeurIPS)*, 2017. URL https://proceedings.neurips.cc/paper_files/paper/2017/hash/8a1d694707eb0fefe65871369074926d-Abstract.html.
- Lukas Hoyer, Dengxin Dai, and Luc Van Gool. Hrda: Context-aware high-resolution domain-adaptive semantic segmentation. In *European Conference on Computer Vision*. Springer, 2022.
- Xueqi Hu, Qiusheng Huang, Zhengyi Shi, Siyuan Li, Changxin Gao, Li Sun, and Qingli Li. Style transformer for image inversion and editing. In *Conference on Computer Vision and Pattern Recognition*, 2022.
- Xun Huang and Serge Belongie. Arbitrary style transfer in real-time with adaptive instance normalization. In *IEEE International Conference on Computer Vision (ICCV)*, 2017. URL https://openaccess.thecvf.com/content_iccv_2017/html/Huang_Arbitrary_Style_Transfer_ICCV_2017_paper.html.
- Xun Huang, Ming-Yu Liu, Serge Belongie, and Jan Kautz. Multimodal unsupervised image-to-image translation. In *European Conference on Computer Vision (ECCV)*, 2018. URL https://openaccess.thecvf.com/content_ECCV_2018/html/Xun_Huang_Multimodal_Unsupervised_Image-to-image_ECCV_2018_paper.html.
- Phillip Isola, Jun-Yan Zhu, Tinghui Zhou, and Alexei A Efros. Image-to-image translation with conditional adversarial networks. In *IEEE Conference on Computer Vision and Pattern Recognition (CVPR)*, 2017. URL https://openaccess.thecvf.com/content_cvpr_2017/html/Isola_Image-To-Image_Translation_With_CVPR_2017_paper.html.
- Tero Karras, Timo Aila, Samuli Laine, and Jaakko Lehtinen. Progressive growing of GANs for improved quality, stability, and variation. In *International Conference on Learning Representations (ICLR)*, 2018. URL <https://arxiv.org/abs/1710.10196>.
- Tero Karras, Samuli Laine, and Timo Aila. A style-based generator architecture for generative adversarial networks. In *IEEE/CVF Conference on Computer Vision and Pattern Recognition (CVPR)*, 2019. URL https://openaccess.thecvf.com/content_CVPR_2019/html/Karras_A_Style-Based_Generator_Architecture_for_Generative_Adversarial_Networks_CVPR_2019_paper.html.
- Tero Karras, Samuli Laine, Miika Aittala, Janne Hellsten, Jaakko Lehtinen, and Timo Aila. Analyz-

- ing and improving the image quality of StyleGAN. In *IEEE/CVF Conference on Computer Vision and Pattern Recognition (CVPR)*, 2020. URL https://openaccess.thecvf.com/content_CVPR_2020/html/Karras_Analyzing_and_Improving_the_Image_Quality_of_StyleGAN_CVPR_2020_paper.html.
- Junho Kim, Minjae Kim, Hyeonwoo Kang, and Kwanghee Lee. U-gat-it: Unsupervised generative attentional networks with adaptive layer-instance normalization for image-to-image translation. *arXiv preprint arXiv:1907.10830*, 2019.
- Soohyun Kim, Jongbeom Baek, Jihye Park, Gyeongnyeon Kim, and Seungryong Kim. Instaformer: Instance-aware image-to-image translation with transformer. In *Conference on Computer Vision and Pattern Recognition, 2022a*.
- Taehyeon Kim, Shinhwan Kang, Hyeonjeong Shin, Deukryeol Yoon, Seongha Eom, Kijung Shin, and Se-Young Yun. Region-conditioned orthogonal 3d u-net for weather4cast competition. *Conference on Neural Information Processing Systems*, 2022b.
- Diederik P. Kingma and Jimmy Ba. Adam: A method for stochastic optimization. In *International Conference on Learning Representations (ICLR)*, 2015. URL <https://arxiv.org/abs/1412.6980>.
- Christian Ledig, Lucas Theis, Ferenc Huszár, Jose Caballero, Andrew Cunningham, Alejandro Acosta, Andrew Aitken, Alykhan Tejani, Johannes Totz, Zehan Wang, et al. Photo-realistic single image super-resolution using a generative adversarial network. In *IEEE Conference on Computer Vision and Pattern Recognition (CVPR)*, 2017. URL https://openaccess.thecvf.com/content_cvpr_2017/html/Ledig_Photo-Realistic_Single_Image_CVPR_2017_paper.html.
- Hsin-Ying Lee, Hung-Yu Tseng, Jia-Bin Huang, Maneesh Singh, and Ming-Hsuan Yang. Diverse image-to-image translation via disentangled representations. In *European Conference on Computer Vision (ECCV)*, 2018. URL https://openaccess.thecvf.com/content_ECCV_2018/html/Hsin-Ying_Lee_Diverse_Image-to-Image_Translation_ECCV_2018_paper.html.
- Boyi Li, Felix Wu, Kilian Q Weinberger, and Serge Belongie. Positional normalization. In *Advances in Neural Information Processing Systems (NeurIPS)*, 2019. URL <https://proceedings.neurips.cc/paper/2019/hash/6d0f846348a856321729a2f36734d1a7-Abstract.html>.
- Jianxin Lin, Yingce Xia, Tao Qin, Zhibo Chen, and Tie-Yan Liu. Conditional image-to-image translation. In *IEEE Conference on Computer Vision and Pattern Recognition (CVPR)*, 2018. URL https://openaccess.thecvf.com/content_cvpr_2018/html/Lin_Conditional_Image-to-Image_Translation_CVPR_2018_paper.html.
- Ming-Yu Liu, Thomas Breuel, and Jan Kautz. Unsupervised image-to-image translation networks. In *Advances in neural information processing systems (NIPS)*, 2017. URL https://proceedings.neurips.cc/paper_files/paper/2017/hash/dc6a6489640ca02b0d42dabeb8e46bb7-Abstract.html.
- Qi Mao, Hsin-Ying Lee, Hung-Yu Tseng, Siwei Ma, and Ming-Hsuan Yang. Mode seeking generative adversarial networks for diverse image synthesis. In *IEEE/CVF Conference on Computer Vision and Pattern Recognition (CVPR)*, 2019. URL https://openaccess.thecvf.com/content_CVPR_2019/html/Mao_Mode_Seeking_Generative_Adversarial_Networks_for_Diverse_Image_Synthesis_CVPR_2019_paper.html.
- Lars Mescheder, Sebastian Nowozin, and Andreas Geiger. Which training methods for GANs do actually converge? In *International Conference on Machine Learning (ICML)*, 2018. URL <https://proceedings.mlr.press/v80/mescheder18a>.
- Takeru Miyato, Toshiki Kataoka, Masanori Koyama, and Yuichi Yoshida. Spectral normalization for generative adversarial networks. In *International Conference on Learning Representations (ICLR)*, 2018. URL <https://arxiv.org/abs/1802.05957>.
- Jheng-Wei Su, Hung-Kuo Chu, and Jia-Bin Huang. Instance-aware image colorization. In *IEEE/CVF Conference on Computer Vision and Pattern Recognition (CVPR)*, 2020. URL https://openaccess.thecvf.com/content_CVPR_2020/html/Su_Instance-Aware_Image_Colorization_CVPR_2020_paper.html.
- Jiashun Wang, Chao Wen, Yanwei Fu, Haitao Lin, Tianyun Zou, Xiangyang Xue, and Yinda Zhang. Neural pose transfer by spatially adaptive instance normalization. In *IEEE/CVF Conference on Computer Vision and Pattern Recognition (CVPR)*, 2020. URL https://openaccess.thecvf.com/content_CVPR_2020/html/Wang_Neural_Pose_Transfer_by_Spatially_Adaptive_Instance_Normalization_CVPR_2020_paper.html.
- Xintao Wang, Ke Yu, Shixiang Wu, Jinjin Gu, Yihao Liu, Chao Dong, Yu Qiao, and Chen Change Loy. ESRGAN: Enhanced super-resolution generative adversarial networks. In *European Conference on Computer Vision (ECCV) Workshops*, 2018. URL https://openaccess.thecvf.com/content_eccv_2018_workshops/w25/html/Wang_ESRGAN_Enhanced_Super-Resolution_Generative_Adversarial_Networks_ECCVW_2018_paper.html.
- Mao Xudong, Li Qing, Xie Haoran, Lau Raymond Y. K., and Wang Zhen. Least squares generative adversarial networks. In *IEEE/CVF International Conference on Computer Vision (ICCV)*, 2017. URL https://openaccess.thecvf.com/content_iccv_2017/html/Mao_Least_Squares_Generative_ICCV_2017_paper.html.
- Dingdong Yang, Seunghoon Hong, Yunseok Jang, Tiangchen Zhao, and Honglak Lee. Diversity-sensitive conditional generative adversarial networks. In *International Conference on Learning Representations (ICLR)*, 2019. URL <https://arxiv.org/abs/1901.09024>.
- Shuai Yang, Liming Jiang, Ziwei Liu, and Chen Change Loy. Unsupervised image-to-image translation with generative prior. In *Conference on Computer Vision and Pattern Recognition*, 2022.

- Han Zhang, Tao Xu, Hongsheng Li, Shaoting Zhang, Xiaogang Wang, Xiaoqi Huang, and Dimitris N Metaxas. StackGAN: Text to photo-realistic image synthesis with stacked generative adversarial networks. In *IEEE International Conference on Computer Vision (ICCV)*, 2017. URL https://openaccess.thecvf.com/content_iccv_2017/html/Zhang_StackGAN_Text_to_ICCV_2017_paper.html.
- Richard Zhang, Phillip Isola, Alexei A Efros, Eli Shechtman, and Oliver Wang. The unreasonable effectiveness of deep features as a perceptual metric. In *IEEE Conference on Computer Vision and Pattern Recognition (CVPR)*, 2018. URL https://openaccess.thecvf.com/content_cvpr_2018/html/Zhang_The_Unreasonable_Effectiveness_CVPR_2018_paper.html.
- Zhifei Zhang, Zhaowen Wang, Zhe Lin, and Hairong Qi. Image super-resolution by neural texture transfer. In *IEEE/CVF Conference on Computer Vision and Pattern Recognition (CVPR)*, 2019. URL https://openaccess.thecvf.com/content_CVPR_2019/html/Zhang_Image_Super-Resolution_by_Neural_Texture_Transfer_CVPR_2019_paper.html.
- Junbo Jake Zhao, Michaël Mathieu, and Yann LeCun. Energy-based generative adversarial network. In *International Conference on Learning Representations (ICLR)*, 2017. URL <http://arxiv.org/abs/1609.03126>.
- Haitian Zheng, Mengqi Ji, Haoqian Wang, Yebin Liu, and Lu Fang. CrossNet: An end-to-end reference-based super resolution network using cross-scale warping. In *European Conference on Computer Vision (ECCV)*, 2018. URL https://openaccess.thecvf.com/content_ECCV_2018/html/Haitian_Zheng_CrossNet_An_End-to-end_ECCV_2018_paper.html.
- Jun-Yan Zhu, Taesung Park, Phillip Isola, and Alexei A Efros. Unpaired image-to-image translation using cycle-consistent adversarial networks. In *Conference on Computer Vision and Pattern Recognition (CVPR)*, 2017. URL https://openaccess.thecvf.com/content_iccv_2017/html/Zhu_Unpaired_Image-To-Image_Translation_ICCV_2017_paper.html.
- lowing color transfer method introduced in Su et al. [2020]. In fig. 16, we transfer the source image colors to the target image (HR and LR), and we use the target LR in the generation process. By comparing the generated image “w/o” and “w/” color transfer, we notice that color does have impact on the generated images in terms of overall texture and evidently colors, a slight impact on the overall structure of the image.
- In fig. 17, we transfer the colors of a unrelated image, to the target image (HR and LR), and we use the target LR in the generation process. We observe that indeed the color does have a slight impact on the generation process.

SUPPLEMENTARY MATERIAL

6 QUALITATIVE RESULTS

We provide additional results on both CelebA-HQ and AFHQ (figs. 18 to 23). On CelebA-HQ, Our method generates diverse samples given the HR source and following the LR target. The network learns to follow the pose of the target LR image due to use of SPAdaIN [Wang et al., 2020], while preserving the source features. We also provide additional comparison with reference guided StarGAN v2 shown in figs. 19 and 20. On AFHQ, we generate images on each domain separately, results are shown in figs. 21 to 23.

7 COLOR ABLATION

To inspect the effect of color on the generation process, we choose to alter the original coloring of the target image, fol-

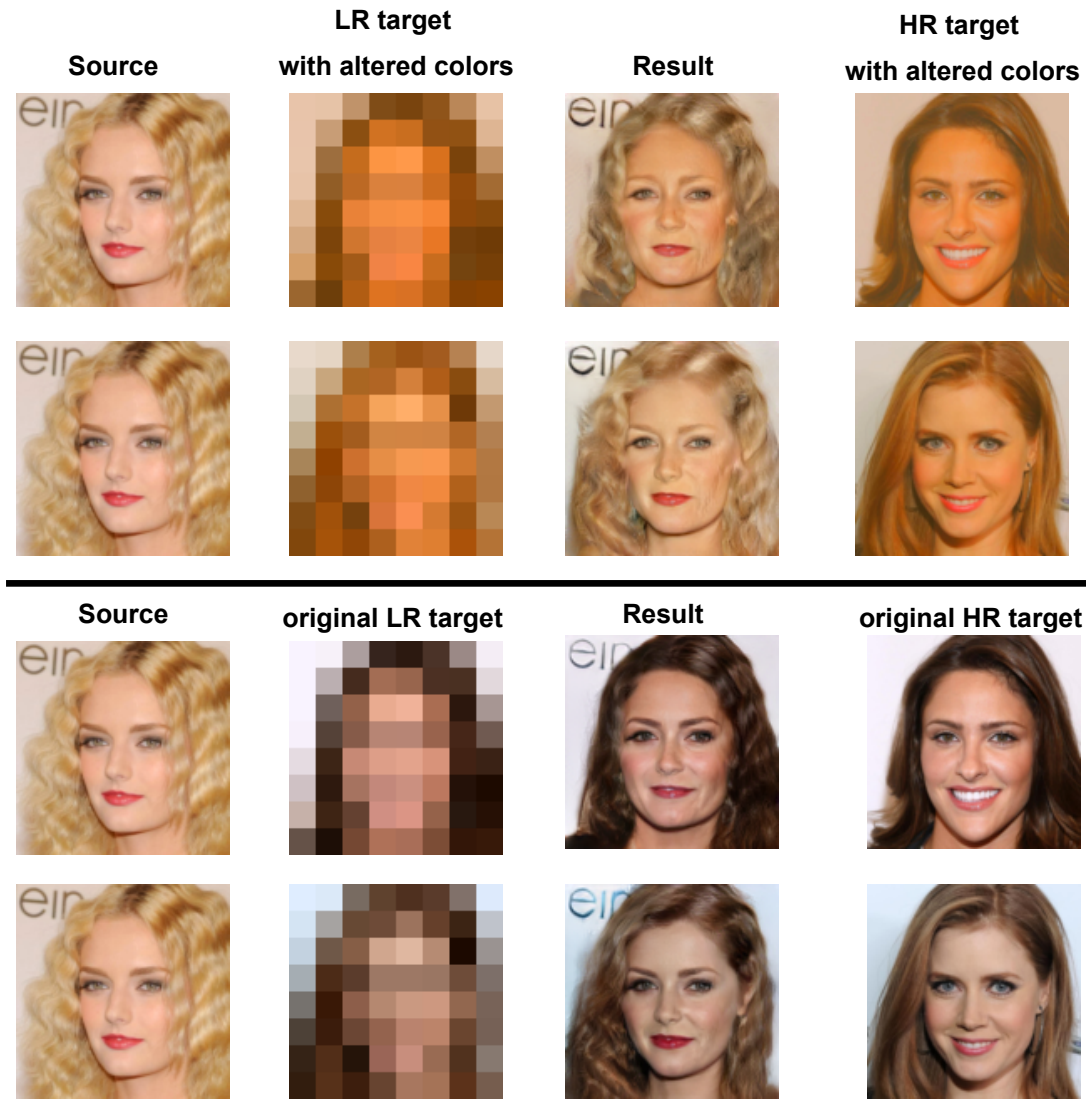


Figure 16: Generated samples on CelebA-HQ [Karras et al., 2018] while modifying the color of LR target using the source image.

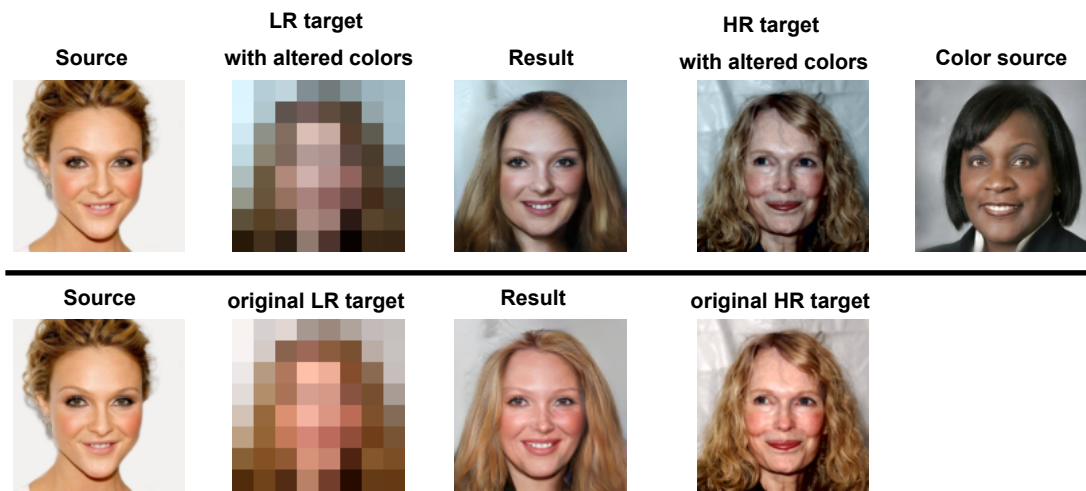


Figure 17: Generated samples on CelebA-HQ [Karras et al., 2018] while modifying the color of LR target using a third image.



Figure 18: Generated samples on CelebA-HQ [Karras et al., 2018] conditioned on HR source (left column) and on the LR target (top row).

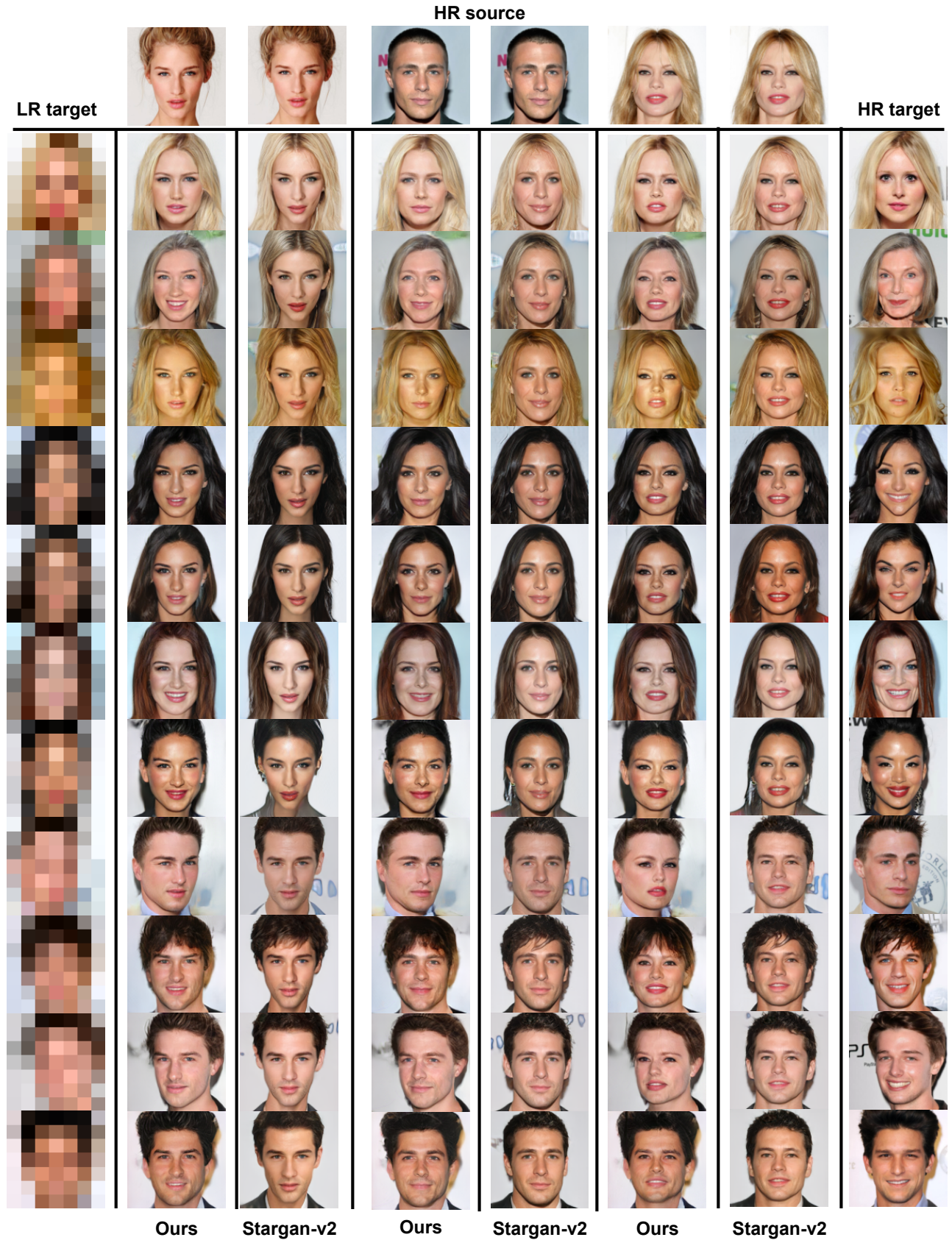


Figure 19: Comparison with StarGAN v2 [Choi et al., 2020] on CelebA-HQ [Karras et al., 2018]. To generate samples, our method uses LR target and HR source while StarGAN v2 uses the HR source and HR target.

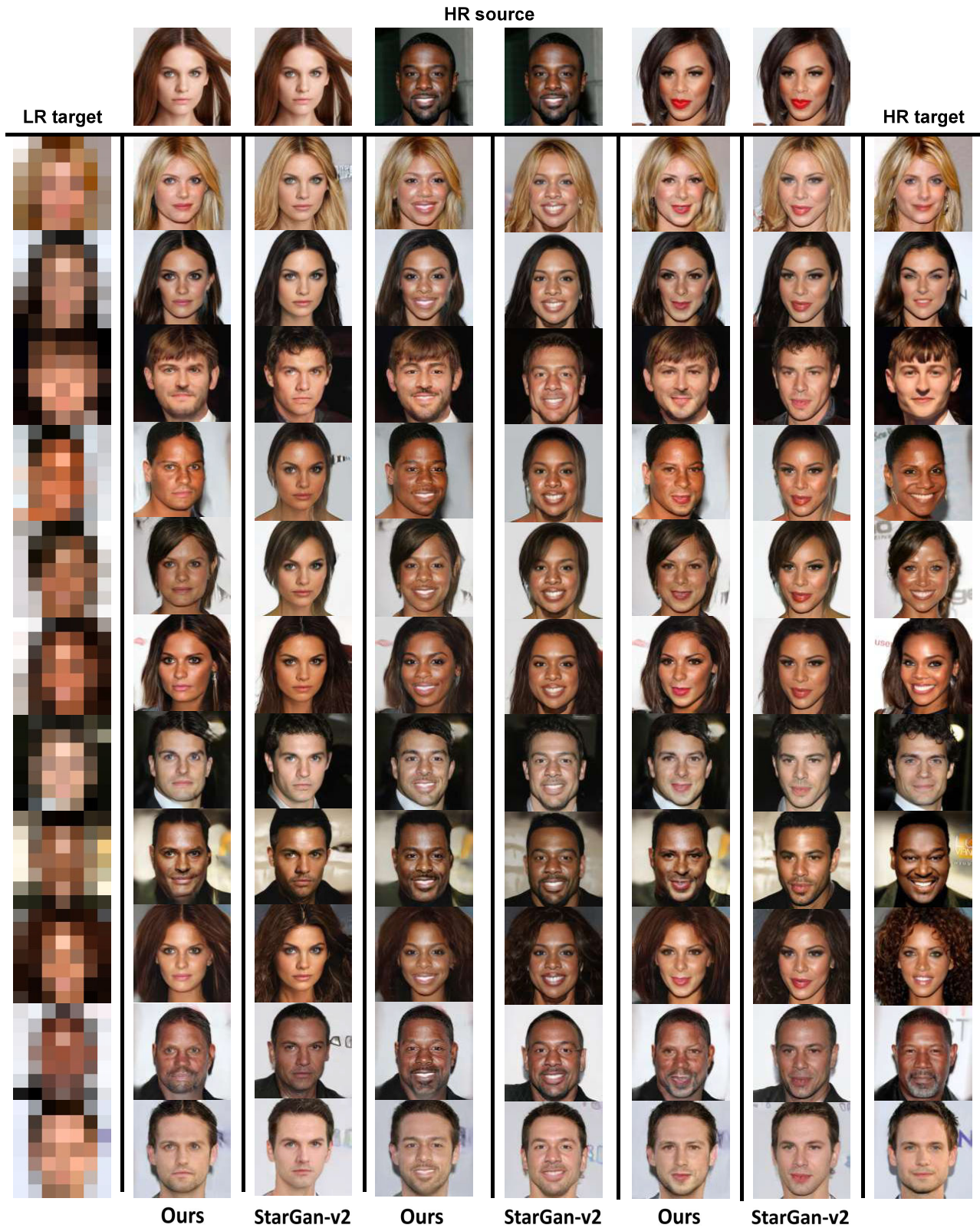


Figure 20: Comparison with StarGAN v2 [Choi et al., 2020] on CelebA-HQ [Karras et al., 2018]. To generate samples, our method uses LR target and HR source while StarGAN v2 uses the HR source and HR target.

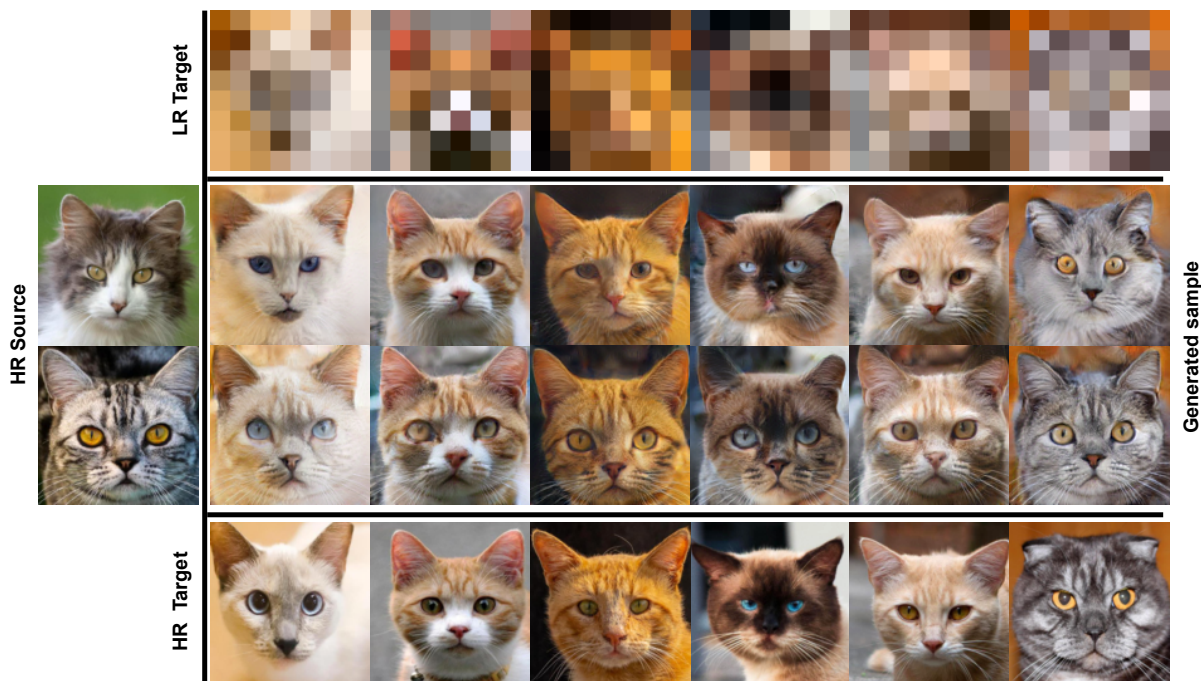


Figure 21: Generated samples on the domain cats of AFHQ [Choi et al., 2018] conditioned on HR source (left column) and on the LR target (top row).

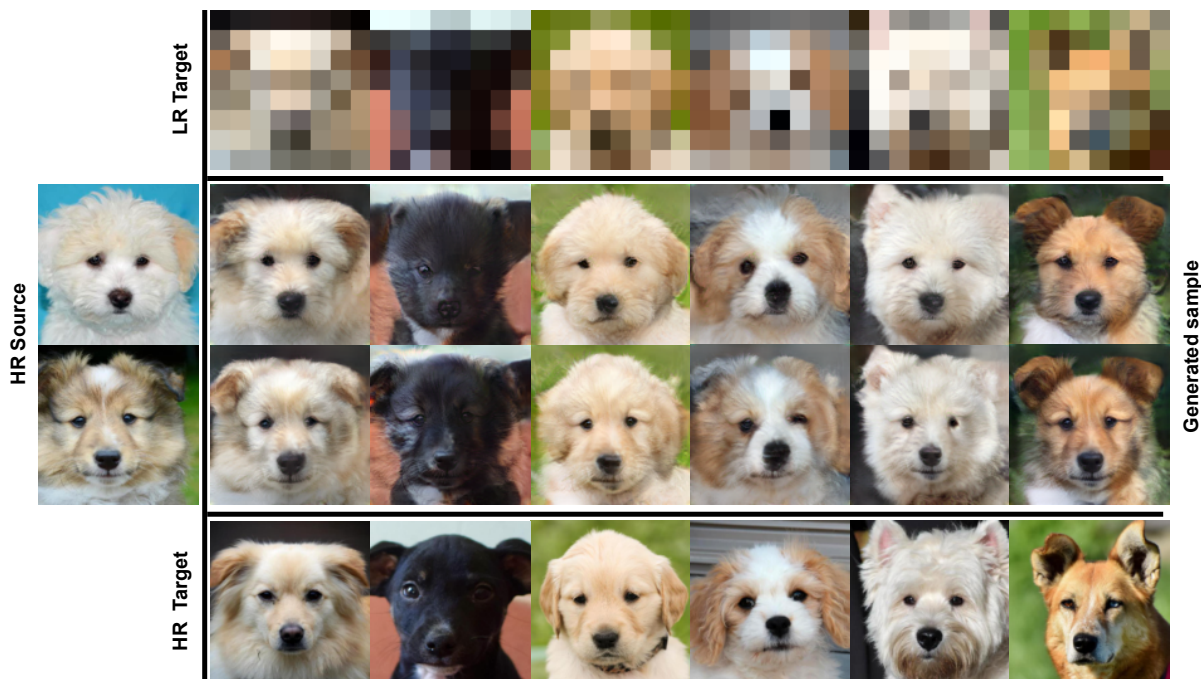


Figure 22: Generated samples on the domain dogs of AFHQ [Choi et al., 2018] conditioned on HR source (left column) and on the LR target (top row).

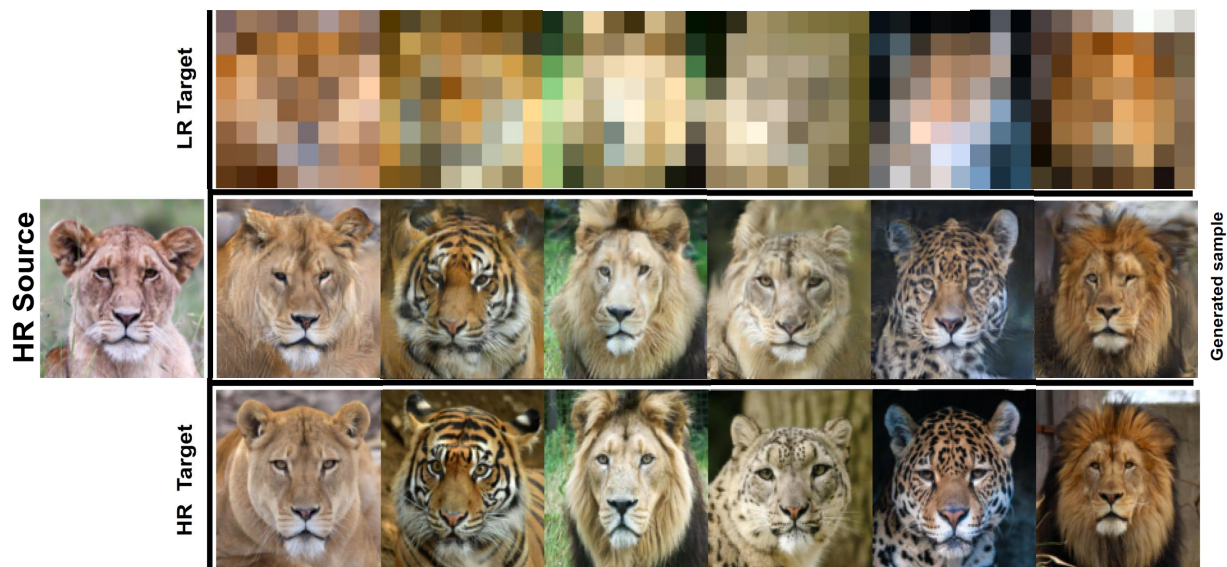


Figure 23: Generated samples on the domain wild of AFHQ [Choi et al., 2018] conditioned on HR source (left column) and on the LR target (top row).